NANO: Brief Reports and Reviews
Vol. 18, No. 3 (2023) 2350011 (9 pages)

DOI: 10.1142/S179329202350011X

World Scientific
www.worldscientific.com

Effect of Doping Sb_2O_3NPs on Morphological, Mechanical, and Dielectric Properties of PVA/PVP Blend Film for Electromechanical Applications

Karar Abdali*, Bahaa H. Rabee†, Ehssan Al-Bermany†, Ali Razzaq Abdulridha†, Khalid Haneen Abass†,§ and Ashraq Mohammed Kadim‡

*Iraq Ministry of Education, Baghdad, Iraq

†Physics Department
College of Education for Pure Sciences
University of Babylon, Babylon, Iraq

‡Medical Physics Department
Hilla University College, Hilla, Iraq
§pure.khalid.haneen@uobabylon.edu.iq

Received 14 August 2022
Accepted 10 January 2023
Published 6 March 2023

In this work, antimony trioxide nanoparticles (Sb_2O_3NPs)-doped polyvinyl alcohol ($PVA_{0.75}$) and polyvinyl pyrrolidone ($PVP_{0.25}$) (i.e., PVAP@$x$$Sb_2O_3$NPs, $x = 0, 0.02$, and 0.04) composite films were prepared using the casting method. Light optical microscopy (LOM), scanning electron microscopy (SEM), and Fourier infrared spectrums (FTIR) were used to investigate PVAP@$x$$Sb_2O_3$NPs films. Sb_2O_3NPs were well dispersed within the matrix. FTIR showed a strong interaction between the matrix material and NPs. The density increased by up to 75% after adding 0.04 wt.% of Sb_2O_3NPs. The mechanical ultrasound properties (MUS) were measured with different ultrasound frequencies in the ranges of (25, 30, 35, 40 and 45 kHz). MUS coefficients such as ultrasonic velocity, absorption coefficient, and bulk modules were significantly improved after the impact of NPs by up to 20%, 115% and 230%, respectively. The reduction of electrical properties such as dielectric and loss constant was associated with an increase in frequency. The dielectric constant of PVAP@Sb_2O_3NPs was increased by about 80% after loading. AC electrical conductivity revealed an improvement with an increase in frequency and loading ratio. The results demonstrate a promising material for electromechanical, energy harvesting, and pressure sensor applications.

Keywords: PVA/PVP; Sb_2O_3NPs; pressure sensor; dielectric properties; energy harvesting.

1. Introduction

The pressure sensor is one of the energy harvesting types that occurs when a material is exposed to external load or mechanical stress.[1] In a nutshell, it is the phenomenon of energy transfer. Pressure sensor or energy harvesting materials have been extensively used in research and electronic and mechanical industries. After being subjected to

§Corresponding author.

mechanical stress, it can convert mechanical energy into electrical energy.[1,2] Polymer nanocomposites (NCs) are distinctive materials with distinct chemical and physical properties. Due to their real potential for a wide range of applications in environmental solutions and the resolution of various environmental issues, these types of NCs have recently received serious attention. The most challenging aspect of NCs is the complicated interface between nanoparticles and the polymer matrix.[3,4] Broad specific surfaces are created due to the small dimensions, emphasizing the significance of polymer–nanoparticle interactions.[5] High-performance properties are essential to investigating and understanding the interpolation process between NPs and the polymer matrix.[6,7]

The chemical structure of polyvinyl alcohol (PVA) is CH_3CHOH $(CH_2–CHOH)_n$. PVA is a water-soluble polymer synthesized from vinyl acetate.[6] It is widely used in various optoelectronic, potential, and dielectric applications. It has weight ranges for different viscosity grades.[8] PVA is well-known for its use in surgical applications, artificial leather, tubing, oil-derivative gaskets with good stability, rubber-like articles, transport belts, emulsifiers, paper and paperboard adhesives, nanomaterials, and other fabrics.[9] It should be water-insoluble as it is processed for textile fibers and other uses.[10] An aqueous solution of sulfuric acid and formaldehyde containing sodium sulfate is used to produce PVA fiber. The hydroxyl groups are converted to formal cyclic groups. A group of researchers analyzed the rheological behavior of an aqueous solution of PVA with various molecular weights and the ratio of percentage weight that had been frozen and thawed.[11,12] Polyvinyl pyrrolidone (PVP) is a white-cultured powder with different vinyl polymers or homopolymers. PVA is stable at various temperatures, and in hygroscopic polymers, and water-soluble polymers. PVP is brittle, transparent, and glassy.[13] Complexes are made up of many different compounds because they are transparent, brittle, and glassy.[14,15]

PVA and PVP are well-known and desirable polymers that are used in the production of optical sensors, optoelectronics, and electronic systems as idealistic and efficient binders.[16] They are extremely appropriate thermodynamically. Their blend interrelates through H bonding between the hydroxyl (OH) of PVA and the carbonyl of PVP. PVA/PVP blends are the commonly used, low-cost, and easily accessible procedures for fabricating novel blends with advanced features for promising optoelectronic purposes.[17]

Due to their many applications, Sb_2O_3NPs defy logic with their behavior and properties, so scientists and researchers have closely studied them.[18] The nanoparticle diameters highly influence the optical properties of Sb_2O_3NPs. The smaller domain of Sb_2O_3NPs almost absorbs light and peaks of about 400 nm, whereas the larger environment increases dispersion and the peaks spread and pass to longer red-shifting wavelengths.[19]

Both polymers were intensively investigated as blended or composite polymers with NPs. To the best of our knowledge, the impact of Sb_2O_3NPs on these materials has not been investigated until today. Therefore, this study was focused on the impact of Sb_2O_3NPs for the first time loaded with different ratios into PVA/PVP blended polymer to fabricate new PVAP@Sb_2O_3NPs films. The resultant films can be used in different optoelectronic, energy harvesting, and mechanical applications.

2. Experimental Section

2.1. *Materials*

PVA (99.9%) powder was provided by DIDACTIC with an 18000 Mw Dalton, 1.19–1.31 g/cm^3 density, and a 200°C melting point. PVP (99.9%) powder was obtained from Central Drug Home with an Mw 40,000 Dalton, 1.2 g/cm^3 density, and a 150–180°C melting point, and Sb_2O_3NPs were purchased from Sigma Aldrich with (20–30) nm average grain size and purity of assay 99.5%.

2.2. *Fabrication of NCs*

The 0.75 g of PVA and 0.25 g of PVP were separately dissolved in 60 mL of deionized water using a magnetic stirrer for 3 h to get a homogeneous solution, and then the mixtures were independently loaded with 0.00 wt.%, 0.02 wt.% and 0.04 wt.% of Sb_2O_3NPs as shown in Table 1. The blending process of Sb_2O_3NPs with PVA/PVP continued for 1 h to achieve a homogeneous mixture at 50°C. The solutions were independently casted into a 5 cm Petri dish and left to dry for eleven days. The obtained films were investigated using LOM, SEM, FTIR, MUS, and LCR meters.

Table 1. Purification methods of samples.

Sample ID	The ratio (wt.%) PVA	PVP	NP	Total mixing time (h)	Drying method
PVA/PVP	0.750	0.250	0.00	3	50 ± 0.5°C under air
PVAP@0.02Sb_2O_3NPs	0.735	0.245	0.02	4	
PVAP@0.04Sb_2O_3NPs	0.720	0.240	0.04	4	

2.3. *Techniques*

The LOM and SEM images were captured using a Nikon, Olympus model 73,346, and SEM, Sigma VP Carl Zeiss, respectively, to investigate the morphological properties. A Bruker FTIR spectrophotometer (Vertex 701) in (4000–400) cm^{-1} was used to study the chemical properties. The SV-DH-7A and SVX-7 systems were used to measure the mechanical properties. An LCR meter (Hi TESTER, HIOKI 3532-50) was used to measure the electrical properties.

3. Results and Discussion

3.1. *LOM and SEM investigations*

Figure 1 represents the LOM images of PVA/PVP blends before and after loading with different ratios of Sb_2O_3NPs at (100×) magnification power. Figure 1(a) shows the homogeneous blend polymers. whereas a diffusion of 0.02 wt.% and 0.04 wt.% of the Sb_2O_3NPs in the blend was represented in the exact figures of (b) and (c) images, respectively. Figures 1(b) and 1(c) illustrate an acceptable homogeneity with uniformed dispersion and some aggregation of the NPs in the blended polymers.[13] In comparison, increasing the loading ratio of the Sb_2O_3NPs from 0.02 wt.% to 0.04 wt.% in the blended polymer revealed significant enhancement and diffusion of the NPS compared with the second sample.

The structure, morphology, and surface fraction of PVAP@$x$$Sb_2O_3$NPs films were explained using SEM, as shown in Fig. 2. Figure 2(a) shows the homogeneous and smooth surface of the blended polymer in agreement with LOM images. The low addition of 0.02 wt.% of Sb_2O_3NPs exhibited a partial dispersion of the NPs in the blend polymer, as revealed in Fig. 2(b). Increasing the loading ratio of Sb_2O_3NPs is associated with better diffusion of Sb_2O_3NPs morphology and surface of the NCs. That could imply the homogeneity of the Sb_2O_3NPs growth mechanism (2c). The average grain size (a_v) of Sb_2O_3NPs was measured on the surface of NCs via SEM. The sizes ranged from a few nanometers to a few microns in some agglomeration regions. The a_v was reflected in the SEM diagram due to the good dispersion of NPs into the blend, agreeing with the literature.[20]

3.2. *FTIR investigations*

Figure 3 exhibits the FTIR spectrum of PVAP@$x$$Sb_2O_3$NPs samples in the IR range of (500–4000) cm^{-1}. The FTIR spectrum of PVA/PVP blended polymers showed excellent compatibility

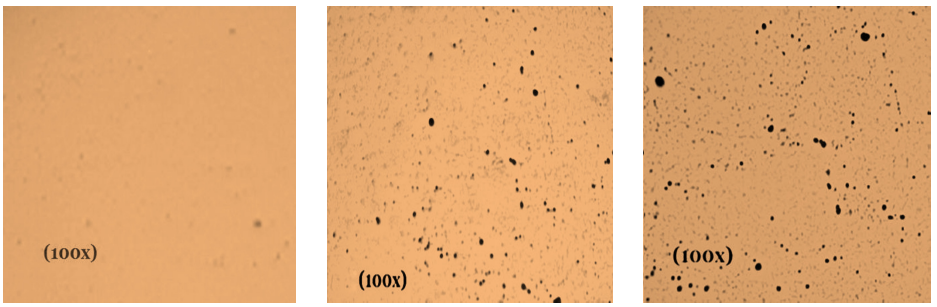

(a) (b) (c)

Fig. 1. LOM images of (a) PVA/PVP, (b) PVAP@0.02Sb_2O_3NPs and (c) PVAP@0.04Sb_2O_3NPs.

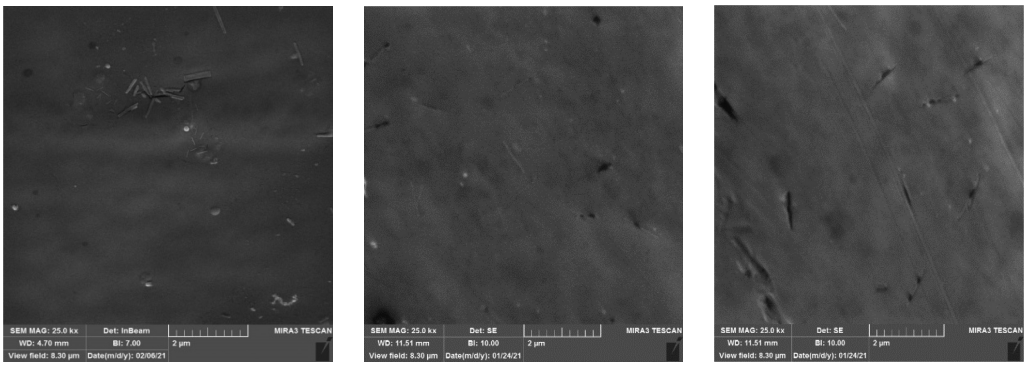

(a) (b) (c)

Fig. 2. SEM images of (a) PVA/PVP, (b) PVAP@0.02Sb_2O_3NPs and (c) PVAP@0.04Sb_2O_3NPs.

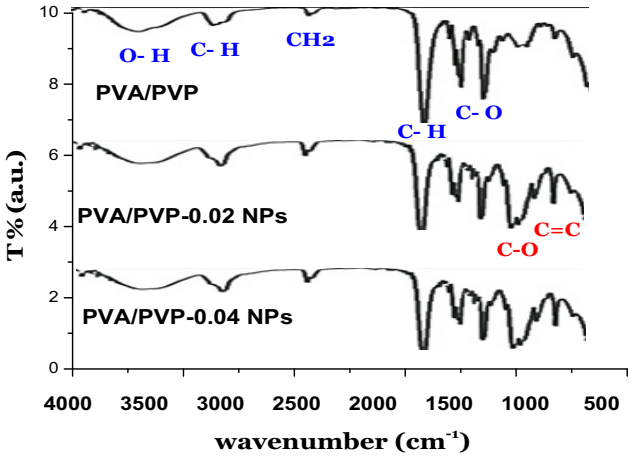

Fig. 3. FTIR spectrum of PVAP@$x$$Sb_2O_3$NPs.

with the functional groups of 3570, 3020, 2450, 1715, 1490, 1330, and weak peaks at 1200 cm^{-1} and 825 cm^{-1} associated with O–H, C–H, CH_2, C=O, C–H, C–O, and C–O, respectively, a functional group in agreement with the literature.[14] In contrast, incorporating Sb_2O_3NPs created a strong interfacial interaction between the blended polymers PVA/PVP and NPs. Adding the Sb_2O_3NPs impacts the position and intensity of the peaks at 3020 cm^{-1} (C–H) and presents new peaks at 1115 cm^{-1} and 825 cm^{-1}. In addition, the intensity of other peaks impacted 2450 cm^{-1}, 1715 cm^{-1} and 1490 cm^{-1} after increasing the loading ratio of the NPs, in agreement with other findings.[21,22] That indicates the strong interfacial interaction formed between the polymers and nanoparticles where H bonding formulation could be created between the C–H groups of PVA and the (C=O) groups of PVP and strongly bonded between the blended polymers and Sb_2O_3NPs.[23,24]

3.3. *Ultrasound mechanical properties*

The density (ρ) of PVAP@$x$$Sb_2O_3$NPs was determined. The formulation cross-linking between the molecules, the density of the polymers and NCs were measured, as shown in Fig. 4. Density increased after increasing the loading ratio of NPs. Increasing the polymer mass in the matrix leads to swelling of the polymer particles through dissolution in distilled water, which results in the characterization of a complex nanostructure with the polymer in the composites. When comparing the results of increasing Sb_2O_3NPs to the results of PVA/PVP, the contribution of Sb_2O_3NPs affected the increase in density values. The density increased by 75% after adding the 0.04 wt. % of Sb_2O_3NPs. The density is calculated by Eq. (1).[25]

$$\rho = \frac{m}{v}, \tag{1}$$

where (m), and (v) mean the weight and volume of the samples, respectively. The (SV-DH-7A/SVX-7) multi-ultrasound frequency meter was used to make realistic MUS measurements at various ranges of frequency (25, 30, 35, 40 and 45) kHz. The MUS

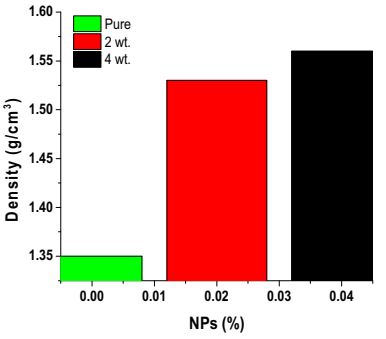

Fig. 4. Density versus NPs wt.%.

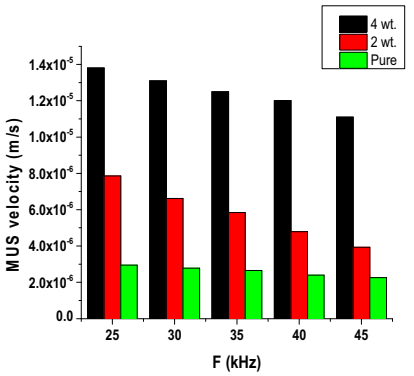

Fig. 5. MUS velocity versus frequency.

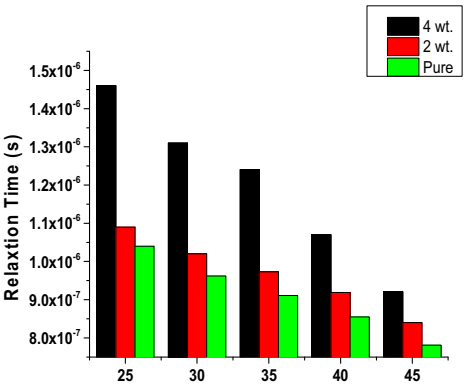

Fig. 6. Relaxation time versus frequency.

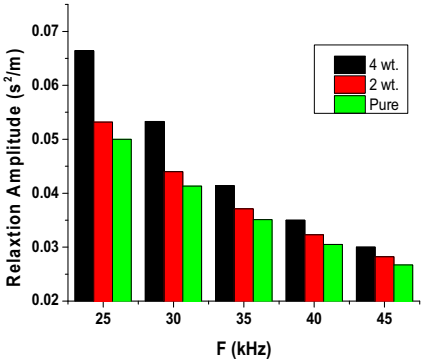

Fig. 7. Relaxation amplitude versus frequency.

waves were applied to examine the samples, pulser, and receiver props. The receiver transforms MUS signals from the electrical sign applied on both sides of props, including a quartz crystal, to generate the mechanical ultrasound wave and named the pulser and receiver. The signal is passed and absorbed through the samples and then received by the receiver that transfers the mechanical ultrasound wave to the electrical sign via digital multi-ultrasound to record the time (t) of passing the MUS mechanical waves. Figure 5 shows the MUS velocity values of PVA/PVP that decreased with the increasing frequency. The MUS velocity was measured using formula (2).[25,26]

$$V = X/t, \tag{2}$$

where (V) is the MUS velocity and (t) is the time of the sample passing of the ultrasound wave. Since the apparent signal in the first channel has a positive peak that reflects the incident MUS wave or initial amplitude (A_o), the negative component in the second channel corresponds to the receiver's amplitude (A) used to calculate the absorption coefficient (α), which was experimentally calculated by contacting the ultrasound meter to the oscilloscope and finding the change in the absorption value of the MUS wave according to Lambert–Beer law in Eq. (3).[25]

$$A = A_o \exp^{(\alpha x)}. \tag{3}$$

This activity is related to structural relaxation, occurring at different frequencies in the associated PVA/PVP and Sb_2O_3NPs composites. A fluid's internal structure is similar to a solid at rest. However, when waves disperse, different periodic forces cause the molecules to flow between vacancies in the lattice during compression and then return to their original position during relaxation.[19,27] Since MUS waves cause an interaction between PVA/PVP and NPs molecules, the velocity is directly proportional to NPs before and after the loading ratio of the NPs but inversely proportional to frequency. MUS waves cause interaction between PVA/PVP and NPs molecules. The velocity improved, whereas the frequency decreased.[20] Figures 6 and 7 show the relaxation time and amplitude (D) that decreased as the frequency increased, which were calculated by applying Eqs. (4) and (6).[28]

$$\tau = \frac{(4\eta_s)}{(3\rho V^2)}, \tag{4}$$

$$D = \alpha / f2'', \tag{5}$$

where (η_s) means liquid viscosity, (τ) means the relaxation time, and (f) means the frequency for mechanical characteristics. The compressibility (β) was measured in the samples using the Laplacian Eq. (6).[25] The fraction between the composition layers was increased by the moment of inertia factor of the PVA/PVP, increasing the loading ratio of the

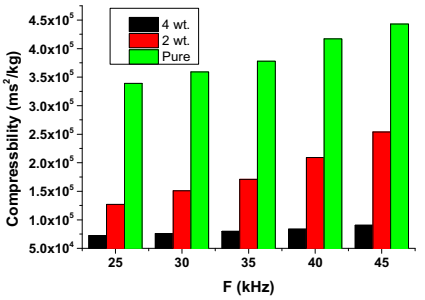

Fig. 8. Compressibility versus frequency.

Sb_2O_3NPs whereas the elasticity modulus (K) was calculated by Eq. (7).[25,28]

$$\beta = (\rho V^2)^{-1}, \tag{6}$$

$$K = \rho V^2. \tag{7}$$

The findings in Fig. 8 show an improvement in the compressibility of PVA/PVP with an increase in frequency. That could be related to the propagation of MUS waves, causing a spontaneous polymer chain conformation. The MUS wave causes compression, impacting and reducing the composition's elasticity.[29] Furthermore, the compressibility of a MUS wave is inversely proportional to its velocity. The bulk modulus decreased as the frequency increased, as seen in Fig. 9. According to Eq. (8),[30] the specific acoustic impedance (Z) of the composite has decreased with increasing frequency, as shown in Fig. 10.

$$Z = \rho V. \tag{8}$$

As compared to velocity, the density is very low. The MUS absorption coefficient is dependent on the frequency value,[26] as shown in Fig. 11, which is also inversely proportional to the frequency.

In general, the nanoparticles strongly impacted and improved the mechanical properties of the samples. That may be related to the strong interfacial

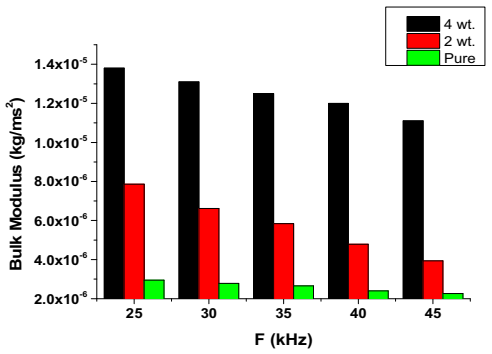

Fig. 9. Bulk modulus versus frequency.

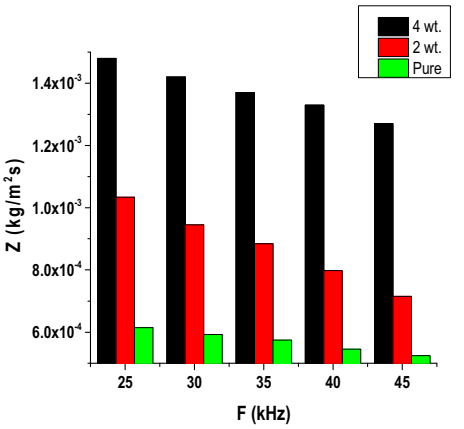

Fig. 10. Z versus frequency.

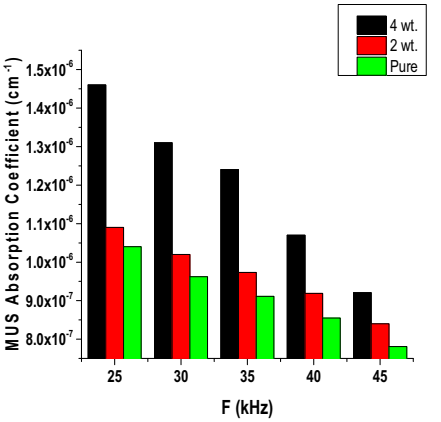

Fig. 11. MUS Absorption coefficient versus frequency.

interaction of the hydrogen bond among the polymers and nanoparticles and filling the gaps between the matrix components and transfer of the load through these connections, in agreement with FTIR findings. Additionally, this led to better reinforcement of the materials and better mechanical properties.

3.4. *AC electrical properties*

The ($\acute{\varepsilon}$), or dielectric constant, is given by Eq. (9). (C_p) is the parallel capacitance, and (C_o) is the vacuum capacitance. The (ε) or dielectric loss is given by formula (10).[31]

$$\acute{\varepsilon} = \frac{Cp}{C''_o}, \tag{9}$$

$$\varepsilon'' = \acute{\varepsilon} D'', \tag{10}$$

where (D) explains the coefficient of dispersion. The variance of ($\acute{\varepsilon}$) and (ε'' against frequency (f) at RT

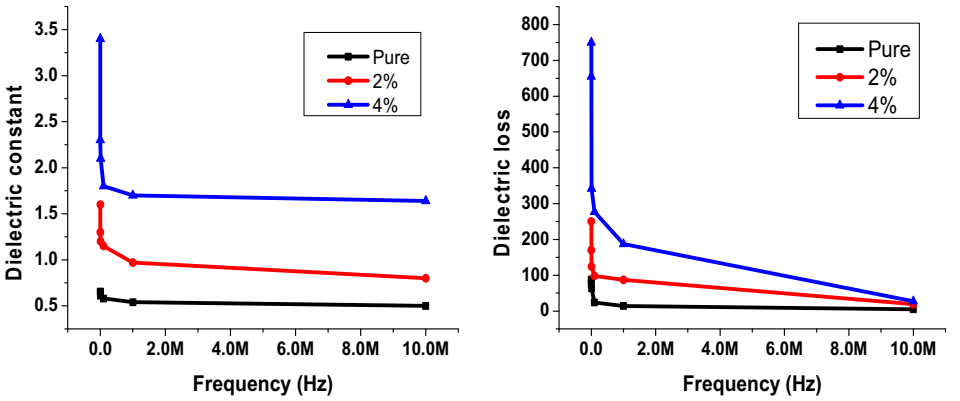

(a) (b)

Fig. 12. The AC characteristics of PVAP@$x$$Sb_2O_3$NPs, (a) The dielectric constant and (b) The dielectric loss.

is shown in Fig. 12. Because of the existence of dipole moments (μ) having enough or suitable time in these regions to order themselves in the direction of the applied electrical field (E), both ε' and ε'' have high values at low (f) values. Furthermore, due to the polarization (P) of space charge (Q), particles or holes collected in the electrode ($p1$) and solution of ions ($p2$), the $p1$ and $p2$ moderators accumulate charge carriers. This improvement in the dielectric parameter raised the frequency, whereas the polarization of Q decreased. More ions cannot propagate in the direction of E because the dielectric properties of the charge carriers (particles or holes) become less effective. This behavior emphasizes non-Debye activity for polymer electrolytes. That cannot obey the field separation at high f values due to a lack of time.[32] Both ε' and ε'' decreased with the increase of Sb_2O_3NPs loading ratio. This result may improve the AC conductivity due to increased PC density. The electrical conductivity was computed by Eq. (11).[31]

$$\sigma_{\mathrm{AC}} = \omega\varepsilon\varepsilon_o'' \tag{11}$$

Figure 13 depicts the electrical conductivity variations of PVAP@$x$$Sb_2O_3$NPs with f. This behavior can be attributed to the interfacial P of the electrical conductivity with increasing the f value.[33] Electrical conductivity values were enhanced with the increasing the Sb_2O_3NPs contents due to the increase in the density of charge carriers.[32,34]

The relationship between the dielectric constant and applied load is illustrated in Fig. 14. The dielectric constant values improved with the increasing applied load and NPs content, and this is related to the responsibility of crystals to the externally

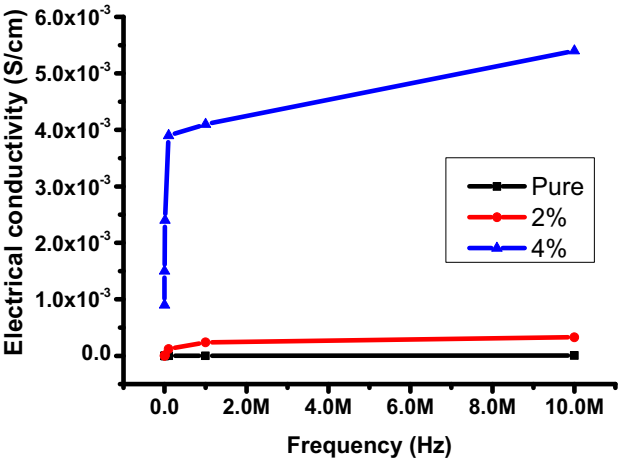

Fig. 13. The AC electrical conductivity versus frequency of PVAP@$x$$Sb_2O_3$NPs films.

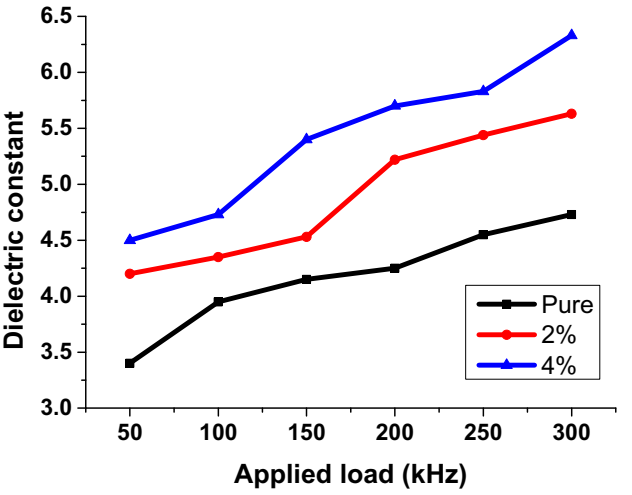

Fig. 14. Dielectric constant versus applied load of PVAP@$x$$Sb_2O_3$NPs films.

applied load and then spontaneously generate the electricity, in agreement with other behavior findings in the literature.[35–40]

4. Conclusions

The PVAP@$x$$Sb_2O_3$NPs films were successfully fabricated using the traditional casting method. The FTIR peaks indicated that the increase of Sb_2O_3NPs content is associated with forming strong interactions, suggesting that Sb_2O_3NPs play a significant role in the conduction process due to the interaction between Sb_2O_3NPs and the hydroxyl group of PVA/PVP. The LOM and SEM images showed an excellent diffusion of Sb_2O_3NPs within the mixture. The MUS and electrical properties of PVAP@$x$$Sb_2O_3$NPs films were noticeably enhanced after loading. MUS properties such as ultrasonic velocity, absorption coefficient, and bulk modules were improved by up to 20%, 115%, and 230%, respectively. This study helped to understand these materials as they were combined for the first time. The AC electrical conductivity of the PVA/PVP blend was increased as the amount of Sb_2O_3NPs increased, with a decrease in the values of dielectric and loss constant. The dielectric constant of the PVA/PVP was increased by about 80% when the applied load increased. As a result, these films are promising materials for use in electromechanical purposes.

References

1. M. Kumar and P. Kumari, *Polym. Bull.* (2022), 10.1007/s00289-022-04275-2.
2. X. F. Liu, C. X. Xiong, H. J. Sun, L. J. Dong, R. Li and Y. Liu, *Mater. Sci. Eng. B: Solid-State Mater. Adv. Technol.* **127**, 261 (2006).
3. M. Anandha Jothi, D. Vanitha, N. Nallamuthu, A. Manikandan and S. Asath Bahadur, *Phys. B: Condens. Matter* **580** (2020).
4. E. Al-Bermany and B. Chen, *Polym. Int.* **70**, 341 (2021).
5. M. Suresh, V. Siva, S. A. Bahadur and S. Athimoolam, *J. Mole. Struct.* **1221**, 128820 (2020).
6. A. J. Al-Zuhairi, A. S. Allw, K. A. Obaid, S. R. Rasool and A. O. Mousa, *J. Eng. Appl. Sci.* **12**, 7800 (2017).
7. M. A. Kadhim and E. Al-Bermany, *J. Compos. Mater.* **55**, 2793 (2021).
8. E. V. Thompson and J. E. Mark, *Polymer Data Handbook*, 2nd ed. (Oxford University Press, Inc, New York, 1999).
9. W. Wang, H. Zhang, Y. Dai, H. Hou and H. Dong, *Iran. Polym. J.* **24**, 687 (2015).
10. S. Feiz, A. H. Navarchian and O. M. Jazani, *Iran. Polym. J.* **27**, 193 (2018).
11. N. Joshi, K. Suman and Y. M. Joshi, *Macromolecules* **53**, 3452 (2020).
12. H. Rafiei, M. Abbasian and R. Yegani, *Iran. Polym. J.* **30**, 769 (2021).
13. K. Abdali, *Silicon* **1** (2022) 10.1007/s12633-022-01678-8.
14. A. K. Al-shammari and E. Al-Bermany, *J. Phys.: Conf. Ser.* **1973**, 012165 (2021).
15. A. A. M. Hassan, K. Abdali, K. Haneen Abass, E. Al-Bermany, F. Sh. Hashim and O. Abdulazeez, *Int. J. Mech. Eng.* **7**, 2 (2022).
16. J. Zhu, Q. Li, Y. Che, X. Liu, C. Dong, X. Chen and C. Wang, *Polymers* **12**, 453 (2020).
17. H. E. Ali and Y. Khairy, *Phys. B Condens. Matter* **570**, 41–47 (2019).
18. S. C. Grund, K. Hanusch, H. J. Breunig and H. U. Wolf, *Ullmann's Encyclopedia of Industrial Chemistry* (Wiley-VCH Verlag, Weinheim, Germany, 2006).
19. V. Siva, D. Vanitha, A. Murugan, A. Shameem and S. A. Bahadur, *Compos. Commun.* **23** (2021).
20. K. Abdali, *Trans. Electr. Electron. Mater.* (2022), 10.1007/s42341-022-00388-7.
21. R. Lamba, A. Umar, S. K. Mehta and S. K. Kansal, *Ceram. Int.* **41**, 5429 (2015).
22. K. Abdali, *J. Mater. Sci. Mater. Electron.* (2022), 10.1007/s10854-022-08676-x.
23. J. Jiang, J. Xie, H. Zhong, F. Dong, N. Liu, W. Tang, H. Zhu and J. Zhang, *J. Alloys Compd.* **818**, 152910 (2020).
24. A. K. H. Al-Khalaf, K. Abdali, A. O. Mousa and M. A. Zghair, *Asian J. Chem.* **31**, 393 (2019).
25. A. J. Bard and L. R. Faulkner, *Ann. Rev. Mater. Sci.* **30**, 117 (1980).
26. A. I. Abdelamir, E. Al-Bermany and F. S. Hashim, *AIP Conf. Proc.* (2020) 020110.
27. K. Abdali Obaid, S. R. Rasool and A. Jassim Al-Zuhairi, *J. Eng. Appl. Sci.* **14**, 6002 (2019).
28. L. W. Schmerr, *Fundamentals of Ultrasonic Nondestructive Evaluation*, 2nd edn. (Springer International Publishing, Cham, 2016).
29. J. Wang, S. Shi, X. Liu, H. Wu, H. Wang, J. Xu, L. Yang and W. Qiu, *J. Mater. Sci. Mater. Electron* (2022), 10.1007/s10854-022-08791-9.
30. L. J. Bond, *Fundamentals of Ultrasonic Inspection* (ASM Handbook, Iowa State University, 2018).
31. H. Hu, F. Zhang, S. Luo, W. Chang, J. Yue and C.-H. Wang, *Nano Energy* **74**, 104844 (2020).
32. S. S. Al-Abbas, R. A. Ghazi, A. K. Al-shammari, N. R. Aldulaimi, A. R. Abdulridha, S. H. Al-Nesrawy and E. Al-Bermany, *Mater. Today: Proc.* **42**, 2469 (2021).

33. D. Coetzee, M. Venkataraman, J. Militky and M. Petru, *Polymers* **12** (2020).
34. K. Abdali, F. Lamis, A. Abdmuslem, O. Abdulazeez and A. Abdulazeez, *J. Glob. Pharma Technol.* **10**, 75 (2018).
35. A. A. Alrehaili, A. F. Gharib, A. El Askary, M. A. El-Morsy, N. S. Awwad, H. A. Ibrahium and A. A. Menazea, *Opt. Mater.* **129** (2022).
36. M. H. Meteab, A. Hashim and B. H. Rabee, *Silicon* (2022), 10.1007/s12633-022-02020-y.
37. S. Zhou, X. Wang, Chen, Z. Huanfu and W. You, *J. Mater. Sci. Mater. Electron.* (2022), 10.1007/s10854-022-08242-5.
38. T. Hera, S. Raza, S. Pragati, P. Raghvendra and S. Prabhakar, *J. Mater. Sci. Mater. Electron.* (2022), 10.1007/s10854-022-08413-4.
39. Z. Xing, J. Weng and C. Ma, *J. Mater. Sci.: Mater. Electron.* **33** (2022).
40. K. Kamal Deep, G. Anamol, S. Nanda and U. Poonam, *J. Mater. Sci: Mater. Electron.* **33** (2022).